

# Low through channel loss wavelength multiplexer using multiple transmission volume Bragg gratings

Shubhashish Datta and Stephen R. Forrest

*Department of Electrical Engineering, Princeton University, Princeton, New Jersey 08544*

Boris Volodin and Vladimir S. Ban

*PD-LD Incorporated, 30B Pennington-Hopewell Road, Pennington, New Jersey 08534*

Received October 6, 2004; accepted January 5, 2005

We describe a wavelength multiplexer design that employs multiple transmission volume Bragg gratings written in the same region of a photosensitive glass having a through channel loss of  $<0.5$  dB. A two-channel multiplexer for wavelengths of  $\lambda = 1310$  and  $1550$  nm is demonstrated to test our design methods and assumptions. Agreement between simulation and experiment is within 0.2 dB at the peak diffraction efficiency. Grating apodization is used to reduce the interchannel cross talk from  $(13.5 \pm 0.5)$  to  $(41.5 \pm 8.5)$  dB, with an experimental through channel loss of  $(0.6 \pm 0.2)$  dB. Effects of angular dispersion on diffraction efficiency and grating spectral shape due to the finite diameter of the incident reading beam are also analyzed. © 2005 Optical Society of America

*OCIS codes:* 050.7330, 230.1360.

## 1. INTRODUCTION

Wavelength multiplexers and combiners are an indispensable part of wavelength division multiplexing schemes that find application in many diverse communication networks and computer interconnects. They have been implemented using arrayed waveguide gratings<sup>1</sup> (AWG), photonic crystals,<sup>2,3</sup> and thin-film filters.<sup>4,5</sup> AWG structures can be used to implement up to 1000-channel multiplexers<sup>1</sup> and are integrable with other photonic devices,<sup>6</sup> although they suffer from a through channel loss of about 3 dB. Photonic crystals<sup>3</sup> exhibit a large through channel loss of 6–7 dB. In contrast, free-space optics devices such as thin-film filters<sup>4</sup> with optical passbands as narrow as 0.2 nm can have very low losses. For example, a four-channel free-space add-drop module<sup>5</sup> has been demonstrated with only 1.1 dB loss. However, a wavelength multiplexer requires the alignment of numerous filters that are packaged with a collimator for each channel in a cascade,<sup>5</sup> whose complexity can lead to unacceptably high costs for many applications.

Here, we present an alternative, low through channel loss free-space-optics wavelength multiplexer concept that comprises isolated or multiple transmission volume Bragg gratings (VBGs) holographically recorded in the same region of a photosensitive glass (Fig. 1). Each wavelength has a corresponding Bragg-matched grating with a unique diffraction angle. The multiwavelength incident light is coupled into the first-order diffraction modes of the corresponding gratings, thereby spatially separating the different wavelengths into their respective channels. The diffracted light is passed through a second Bragg-matched grating section such that the output direction coincides with that of the input. Since the gratings can be

simultaneously recorded by using a phase mask, the alignment and packaging problems faced by thin-film filters are reduced. It is possible to route different channels in this VBG chip into a fiber ribbon, obviating the need for individual optical collimators. Multiplexers with a similar design employing multiple reflection gratings have been demonstrated to have less than 0.5 dB through channel loss.<sup>7</sup>

In this paper, we explore the design principles of VBG-based wavelength multiplexers and compare the performance of both multiplexed and isolated grating structures (Fig. 1). The transmission gratings are modeled using coupled-mode theory<sup>8,9</sup> and are expressed in a transmission matrix formalism that facilitates the analysis of apodized gratings. Advantages of apodization and beam dispersion effects are also discussed. We demonstrate a two-channel wavelength multiplexer by using the multiplexed grating in photorefractive doped silicate glass<sup>10–13</sup> operating at wavelengths of  $\lambda_1 = 1310$  and  $\lambda_2 = 1550$  nm; the demonstration verifies our model predictions.

## 2. MODELING OF MULTIPLEXED GRATINGS

To describe multiple gratings with independent apodization, we divide the gratings into slices along the propagation direction within which the index contrast of each grating is assumed constant. A transmission matrix that describes the power coupled between the various modes by the gratings then represents each slice. The transmission matrix formulation allows for grating reconstruction similar to the discrete layer-peeling algorithm used for modeling reflection gratings.<sup>14</sup>

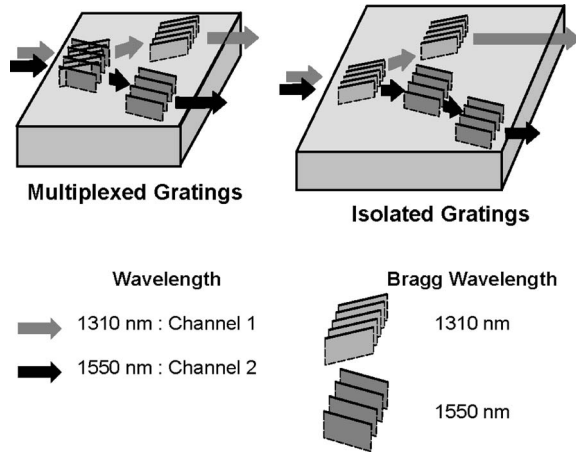


Fig. 1. Structure of two-channel wavelength multiplexers employing (a) multiplexed and (b) isolated gratings.

Consider a multiple-grating structure where energy is coupled between  $N$  modes. The complex fields of each of these modes,  $R^{(i)}(z)$ , at a propagation distance,  $z$ , can be represented as a combination of  $N$  spatial components along the propagation direction with complex spatial frequencies,  $\gamma_i$ , and corresponding amplitudes,  $r_l^{(i)}$ . That is,

$$R(z) = \begin{bmatrix} R^{(1)}(z) \\ R^{(2)}(z) \\ \vdots \\ R^{(N)}(z) \end{bmatrix} = \begin{bmatrix} r_1^{(1)} & r_2^{(1)} & \cdots & r_N^{(1)} \\ r_1^{(2)} & r_2^{(2)} & \cdots & r_N^{(2)} \\ \vdots & \vdots & \ddots & \vdots \\ r_1^{(N)} & r_2^{(N)} & \cdots & r_N^{(N)} \end{bmatrix} \begin{bmatrix} \exp(\gamma_1 z) \\ \exp(\gamma_2 z) \\ \vdots \\ \exp(\gamma_N z) \end{bmatrix} = r \exp(\gamma z). \quad (1)$$

When expressed in terms of its initial value  $R(0)$ , the complex field vector is  $R(z) = T(z)R(0) = (\sum_{l=1}^N T_l \times \exp(\gamma_l z))R(0)$ , where  $T_l$  represents the coefficients of the spatial components of the transmission matrix,  $T(z)$ . Consider the matrix,  $M$ , that describes the coupling between the various modes. Then the diagonal matrix elements are  $M_{ii} = -j\nu^{(i)}/c^{(i)}$ , and the off-diagonal elements are  $M_{ij} = -j\kappa^{(i,j)}/c^{(i)}$ . Here, the modes are characterized by their dephasing constant,  $\nu^{(i)} = (\beta^2 - |\vec{k}^{(i)}|^2)/2\beta$ , and the components of the normalized propagation constant along the propagation direction are  $c^{(i)} = \vec{k}^{(i)} \cdot \hat{z}/\beta$ , where  $\vec{k}^{(i)}$  are the modal propagation constants and  $\beta = 2\pi/\lambda$ .<sup>12</sup> The modes are characterized by their diffraction orders,  $n_g^{(i)}$ . Then the modal propagation constants are defined as  $\vec{k}^{(i)} = \vec{k}_0 - \sum_g n_g^{(i)} \vec{K}_g$ , where  $\vec{k}_0$  is the propagation constant of the incident light and  $\vec{K}_g$  characterizes the  $g$ th grating.

The off-diagonal components of  $M$  are proportional to  $\kappa^{(i,j)}$ , each of which denotes the coupling constant from the  $i$ th and  $j$ th grating modes, and vanishes if no such coupling exists. The elements of the complex vector,  $\gamma$ , are given by the eigenvalues of  $M$ . Let the eigenvectors of  $M$  be denoted by the column vectors,  $e_l$ . Define vectors  $f_l$  as normal to the surface containing the other  $N-1$  eigenvectors, such that  $f_l e_m^T = \delta_{l,m}$ , where  $\delta_{l,m}$  is the Kronecker delta function. Then the singular,  $N$ -dimensional projection coefficient matrices,  $T_l$ , are given by  $T_l = e_l f_l^T$ . The transmission matrix thus defined is computed for different wavelengths and is parameterized by the grating

attributes—coupling constants, orientation, apodization functions, Bragg wavelength, and length.

### 3. WAVELENGTH MULTIPLEXER DESIGN

Here, the design principles for a two-channel wavelength multiplexer operating at wavelengths of  $\lambda = 1310$  and  $1550$  nm are discussed by way of an example that can be generalized for more channels as required. All results consider second-order modes to achieve an accurate estimate of the diffraction efficiencies of the first-order modes. Ignoring the second-order modes leads to a maximum variation of 1% in the results mentioned here. Each channel comprises two identical Bragg-matched gratings, one of which is multiplexed with gratings for the adjacent channel (Fig. 1). A normal angle of incidence is assumed unless stated otherwise. The design parameters to be determined are the length, diffraction angle, and index contrast of each unapodized grating. We begin by fixing the length of the gratings to 3 mm. Shorter gratings are more compact but require a larger diffraction angle and index contrast to maintain the required diffraction efficiency. The sum of the index contrast of each grating should not exceed the saturation value, or the dynamic range, of the photosensitive material.<sup>13</sup> Index saturation adversely affects the grating performance, leading to higher-order spatial harmonics in the index profile. Thus, the dynamic range of the photosensitive material and the dimensions of the device, also constrained by practical packaging requirements, play an important role in fixing the length of the grating. Here a photorefractive glass with a dynamic range for index writing of  $\Delta n = 0.002$  is considered (see Section 4).<sup>13</sup>

The diffraction angles are chosen such that the peaks of the wavelength responses (at  $\lambda = 1310$  and  $1550$  nm) of the two gratings, considered separately, are aligned to the first nulls of the other to minimize interchannel cross talk (Fig. 2, dashed curves). In this case, a broad spectral pass-band is desired. In general, choosing higher-order nulls

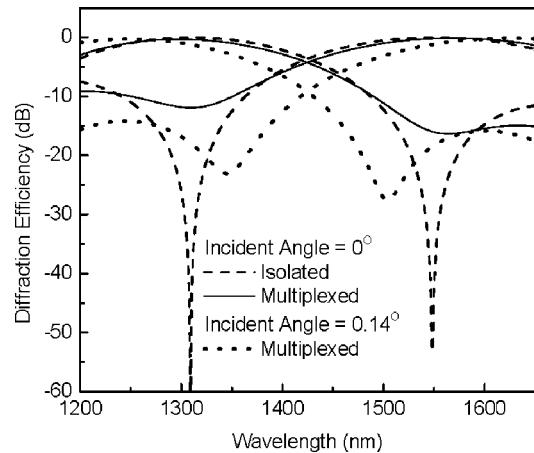


Fig. 2. Wavelength response of two isolated (dashed curves) gratings is compared with that of multiplexed gratings at  $0^\circ$  (solid curves) and  $0.14^\circ$  (dotted curves) angles of incidence. The 3 mm long gratings are Bragg matched to wavelengths of  $\lambda = 1310$  and  $1550$  nm, with diffraction angles of  $2.3^\circ$  and  $-2.55^\circ$ , respectively. The grating index contrasts are  $\Delta n = 0.00044$  and  $0.00052$ , respectively.

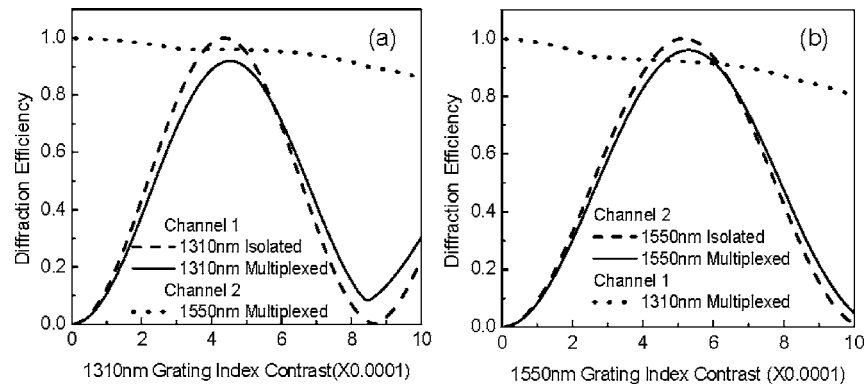


Fig. 3. Dependence of diffraction efficiency of isolated (dashed curves) and multiplexed (solid and dotted curves) gratings on index contrast for the gratings in Fig. 2.

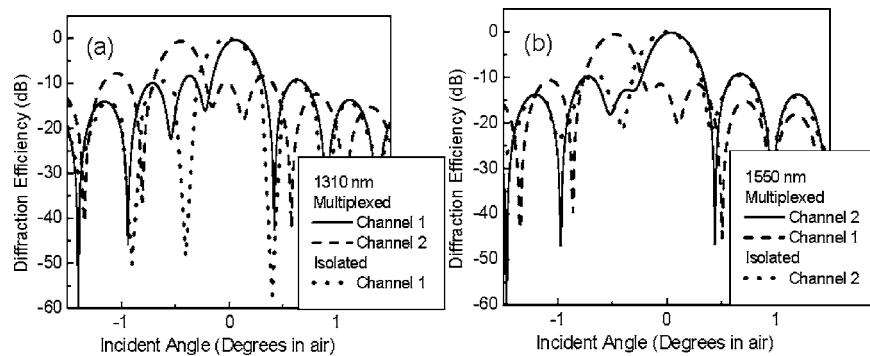


Fig. 4. Dependence of diffraction efficiency of isolated (dotted curves) and multiplexed (solid and dashed curves) gratings on incident angle for the gratings in Fig. 2.

reduces the cross talk, as well as the passband. With this criterion, the diffraction angles for the gratings tuned to  $\lambda=1310$  and  $1550$  nm are found to be  $2.3^\circ$  and  $-2.55^\circ$ , respectively.

The optimal index contrasts of the two multiplexed gratings are adjusted to maximize the diffraction efficiencies of both channels. In Fig. 3, the dependence of the diffraction efficiencies of the multiplexed gratings (solid and dotted curves) on the grating index contrasts are compared with that of single, independent gratings (dashed curves). The optimum index contrasts that maximize the diffraction efficiency of channel 1 at  $\lambda_1=1310$  nm and channel 2 at  $\lambda_2=1550$  nm are  $\Delta n=0.00045$  and  $0.00053$ , respectively. Their sum is well within the dynamic range of the photosensitive glass<sup>13</sup> that is used in the experiment in Section 4.

We next consider the effect of the index contrast on the grating Bragg matched to  $\lambda_1=1310$  nm [Fig. 3(a)]. The response of channel 1 (solid curve) is similar to that of a single grating (dashed curve), the latter having an optimal index contrast of  $\Delta n=0.00044$ . A more significant effect of multiplexing is the reduction of diffraction efficiency from 100% to 92%. This can also be seen when we consider the effect of grating contrast on the response of channel 2 at  $\lambda_2=1550$  nm (dotted curve). As the grating matched to  $\lambda_1$  is made stronger, the diffraction efficiency drops steadily from 100%, which signifies a small dephasing of the gratings in the non-Bragg-matched situation. In this case, the grating diffraction angle should be increased to reduce the amount of light coupled by gratings

into their corresponding first-order modes. Unfortunately, this requires a larger grating index contrast, which may not be possible in all cases owing to the limited dynamic range of the photosensitive material and the number of channels in the multiplexer. Multiplexing also brings with it an inherent asymmetry. For example, the grating tuned to  $\lambda_2$  has smaller dephasing at  $\lambda=1310$  nm and thus couples more light out of channel 1. Hence, the reduction of peak diffraction efficiency at shorter wavelengths is always larger (Fig. 3, solid curves).

Another unwanted effect of multiplexing is the inevitable increase in interchannel cross talk (see Fig. 2). The multiplexed channels (solid curves) do not have the sharp nulls seen in isolated gratings (dashed curves). This increases the cross talk from  $-53$  and  $-67$  dB to  $-16$  and  $-12$  dB for the  $\lambda=1310$  and  $1550$  nm channels, respectively. For example, consider the response of channel 1. Each grating was designed such that its wavelength response exhibits a null at the Bragg wavelength of the other when they are not combined. Hence, the length of the grating tuned to  $\lambda_1=1310$  nm is optimal when the resonance between the zeroth- and first-order diffraction modes allows for complete energy transfer between them for that propagation distance. Ignoring higher-order modes, one can therefore represent each lossless grating channel as an undamped oscillator. When such a grating is multiplexed with the  $\lambda_2=1550$  nm tuned grating whose first-order diffraction mode is strongly coupled to the zero-order mode due to Bragg matching, the two oscillators corresponding to both channels are coupled. Since the

characteristic propagation lengths of the two channels are different, channel 1 exchanges energy with channel 2 off resonance, thereby eliminating the sharp null in the latter.

This effect can also be seen in the dependence of diffraction efficiency on incident angle, in Fig. 4. The response of channel 1 when combined with channel 2 [Fig. 4(a), solid curve] does not exhibit a null at  $-0.4^\circ$  incidence, as observed for a single grating [Fig. 4(a), dotted curve], where channel 2 is strongly coupled [Fig. 4(a), dashed curve]. A similar effect exists at  $0^\circ$  incidence angle, suggesting that cross talk is angle dependent, as expected. However, varying the incidence angle (Fig. 2, dotted curves) is accompanied by a penalty in peak diffraction efficiency.

The cross talk can be significantly reduced by apodizing the grating index contrast profiles. The wavelength response of two 5 mm long isolated gratings tuned to  $\lambda = 1310$  and  $1550$  nm with a Gaussian apodization of width 3 mm (Fig. 5, dashed curves) have improved sideband suppression compared with similar unapodized gratings

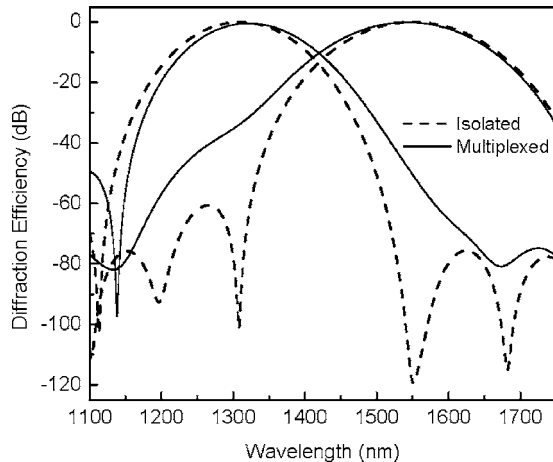


Fig. 5. Wavelength response of isolated (dashed curves) gratings is compared with that of multiplexed gratings (solid curves) at normal incidence. The 5 mm long gratings are Bragg matched to wavelengths of  $\lambda = 1310$  and  $1550$  nm, with diffraction angles of  $1.8^\circ$  and  $-1.9^\circ$ , respectively. The grating index contrasts are Gaussian apodized with a width of 3 mm and have peak values of  $\Delta n = 0.0005$  and  $0.0006$ .

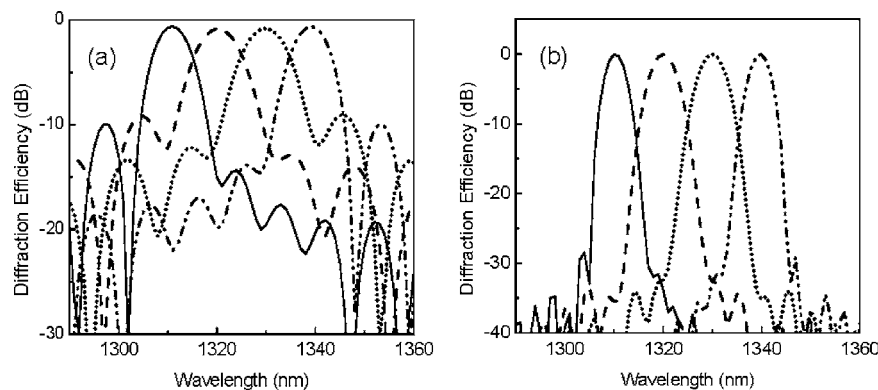


Fig. 6. Wavelength response of a four-channel multiplexer operating at wavelengths of  $\lambda = 1310$ ,  $1320$ ,  $1330$ , and  $1340$  nm. (a) The 4.3 mm long unapodized gratings with index contrast  $\Delta n = 0.0003$  are compared with (b) 7.5 mm wide Gaussian apodized gratings with index contrast  $\Delta n = 0.0002$ . Both sets of gratings have diffraction angles of  $6.7^\circ$ ,  $6^\circ$ ,  $-6^\circ$ , and  $-6.7^\circ$ .

(Fig. 2, dashed curves). The gratings have diffraction angles of  $1.8^\circ$  and  $-1.9^\circ$  and peak index contrast values of  $\Delta n = 0.0005$  and  $0.0006$ , respectively, which are comparable to the parameters of the unapodized gratings shown in Fig. 2. As a result, the multiplexed apodized gratings (Fig. 5, solid curves) exhibit reduced cross talk ( $-33$  and  $-50$  dB) when compared with their unapodized counterparts (Fig. 2, solid curves). A peak diffraction efficiency of  $(-0.23 \pm 0.18)$  dB is achieved. The nulls in the apodized gratings depend on the choice of grating lengths and diffraction angles and are reduced in depth when multiplexed owing to the off-resonance coupling between adjacent channels. Thus, the cross talk in the multiplexed gratings is defined primarily by the Fourier transform of the apodization functions. All these limitations are absent when isolated gratings are used (Fig. 1), the disadvantage of this approach being increased size.

The response of a four-channel wavelength multiplexer operating at  $\lambda = 1310$ ,  $1320$ ,  $1330$ , and  $1340$  nm is shown in Fig. 6(a) and illustrates the extension of the design to multiple channels. In this simulation, the unapodized gratings are 4.3 mm long, with index contrasts of  $\Delta n = 0.0003$ ,  $0.0003$ ,  $0.00031$ , and  $0.00031$  and diffraction angles of  $6.7^\circ$ ,  $6^\circ$ ,  $-6^\circ$ , and  $-6.7^\circ$ , respectively. The  $\lambda = 1320$  and  $1330$  nm center channels have a loss of 0.8 dB, which is slightly higher than that of the other channels (0.6 dB loss) owing to the proximity of the two adjacent channels to the two center channels. A cross talk of  $(-12.8 \pm 0.5)$  dB is achieved, which is comparable to the two-channel multiplexer in Fig. 2. The cross talk is reduced to  $(-34 \pm 1.5)$  dB when the gratings with index contrast of  $\Delta n = 0.0002$  and a Gaussian apodization of width 7.5 mm were used [Fig. 6(b)]. The grating diffraction angles were the same as those of the four-channel multiplexer in Fig. 6(a).

#### 4. EXPERIMENT

A variety of photosensitive media has been considered for volume hologram recording, including inorganic photosensitive silicate glasses,<sup>10–13</sup> lithium niobate,<sup>15,16</sup> photopolymers,<sup>17</sup> and chalcogenide films.<sup>15</sup> Here we consider photosensitive silicate glasses doped with ionic salts containing mixtures of trace amounts of Ag, Ce, F, and Br.<sup>10–13</sup> Details regarding the chemistry and processing of

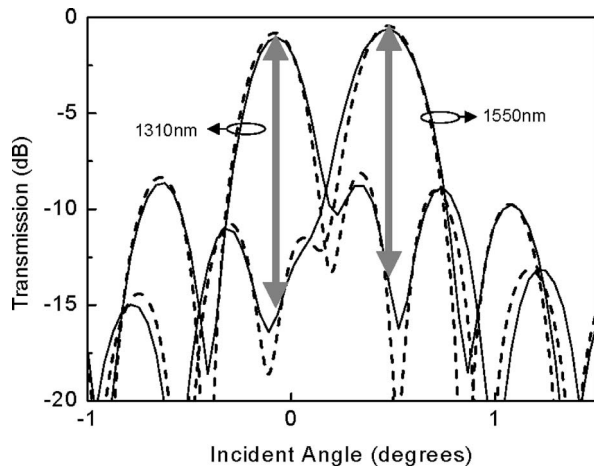


Fig. 7. Experimental (solid curves) and simulated (dashed curves) angular responses of a two-channel wavelength multiplexer written in photosensitive glass with the gratings tuned to wavelengths of  $\lambda=1310$  and  $1550$  nm. The multiplexer comprises 3 mm long grating segments with diffraction angles of  $3^\circ$ . A peak diffraction efficiency of  $>80\%$ , cross talk of  $(-13.5 \pm 0.5)$  dB, and side-mode suppression of 8 dB were observed. Agreement between simulation and experiment is within 0.2 dB at the peak diffraction efficiency.

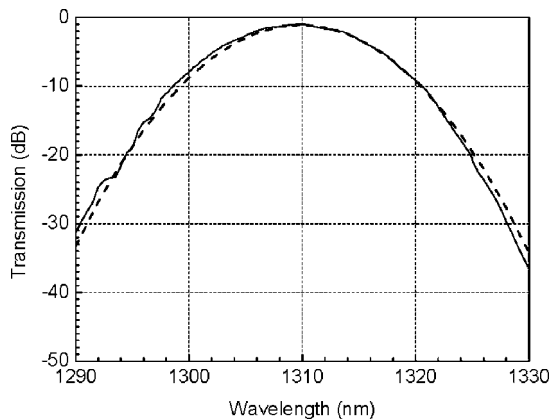


Fig. 8. Experimental (solid curve) and simulated (dashed curve) responses of an apodized grating operating at a wavelength of  $\lambda=1310$  nm achieve a peak diffraction efficiency of  $-1.1$  dB. The apodization function is a Gaussian function of 2 mm width.

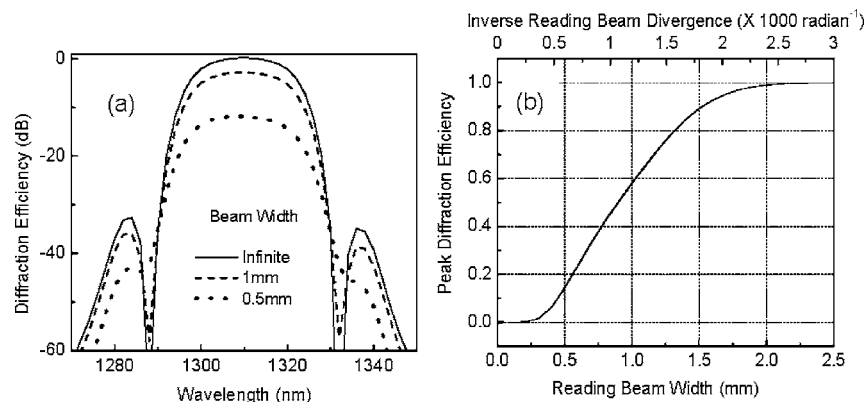


Fig. 9. (a) Simulated response for an apodized transmission grating for reading beams with different spot sizes. (b) The dependence of peak diffraction efficiency versus reading beam diameter and increasing beam divergence is apparent in the figure.

the glass have been previously described.<sup>11,13</sup> The gratings are written in the glass using a photothermorefractive process that involves exposure to a sinusoidal interference pattern followed by heat treatment.<sup>13</sup> During exposure, the output of the writing laser is passed through a beam expander and then split into two beams that interfere on the glass sample, thereby forming the grating. The refractive index of the unexposed glass is 1.49. Following UV exposure at  $\lambda=330$ – $360$  nm, the glass is heat treated at  $450$ – $500$  °C with further heating to  $520$  °C for 3 to 5 h to allow for the formation of a second phase consisting of elongated pyramidal Ag–NaF and Ag–NaBr complexes.<sup>10</sup> The refractive index of NaF is 1.32, and hence the formation of the second phase containing a low density of the alkali halide complexes results in the local reduction of the refractive index. The glass is thermally stable up to  $400$  °C and is insensitive to humidity. Refractive index variations of up to  $\Delta n=0.002$  (corresponding to the dynamic range) can be achieved by this exposure process. A large index contrast is essential for recording multiple gratings and ultimately limits the number of channels in the wavelength multiplexer, as discussed in Section 3. The resolution of the material is sufficiently high to permit the writing of gratings with spatial frequencies of at least  $2500$   $\text{mm}^{-1}$ .<sup>10</sup>

The grating segments of the example two-channel wavelength multiplexer at  $\lambda=1310$  and  $1550$  nm were 3 mm long and were designed for a diffraction angle of  $3^\circ$  in the glass. The index contrast of both gratings was  $\Delta n=0.00045$ , and the sum of the contrasts of the gratings was well within the dynamic range of the material.<sup>13</sup> Isolated gratings with Gaussian apodization were also made.

## 5. RESULTS

The power in one output channel of the wavelength multiplexer was monitored as the angle of incidence was varied to produce the filter transfer functions shown in Fig. 7, with the mirror image function appearing at the second output. Peak diffraction efficiencies of 80% and 87% and a cross talk of  $(-13.5 \pm 0.5)$  dB with a side-mode suppression of approximately 8 dB were experimentally observed for the two channels (solid curves). Agreement between the experimental and the simulation results (dashed curves) is within 0.2 dB at the peak diffraction, which is consis-

tent with model predictions. The nulls in the calculation are smoothed owing to unwanted grating apodization and dispersion due to the finite spot size of the writing and reading beams, respectively, effects ignored in the simulations. A single independent grating with a Gaussian amplitude apodization showed a side-mode suppression of over 30 dB (Fig. 8, solid curve) and a peak diffraction efficiency of  $-1.1$  dB, which reasonably matches the theoretical predictions (dashed curve). These gratings had  $6^\circ$  diffraction angle and 5 mm thickness and therefore had a smaller spectral passband width than the gratings in Fig. 7. The through channel loss measured for these components was  $(0.6 \pm 0.2)$  dB, also consistent with calculation.

## 6. DISCUSSION AND CONCLUSIONS

Writing multiple simultaneous gratings in the same region of the glass reduces the peak diffraction efficiency and increases cross talk due to the power coupled into non-Bragg-matched modes. To minimize these effects, gratings with large diffraction angles and photosensitive material with a large dynamic range are required. Wavelength multiplexers in which gratings are not combined is one possible solution, as shown in Fig. 1. However, apodization can improve the performance of the multiplexed gratings lacking a sharp resonance by allowing the wavelength response to fall sharply as the detuning is increased. As a result, the increase in cross talk due to coupling from neighboring channels is also reduced. Moreover, as aligning sharp nulls to the peaks is not needed, the design tolerance increases, especially for multiplexers with a large number of channels.

Finally, the effects of the reading beam spot size have been analyzed. The grating response for a finite Gaussian beam is approximately the convolution of its Fourier transform, also a Gaussian, and its response to an infinite plane wave. Hence, a smaller spatial beam width increases the beam spread in Fourier space. This approximation is valid as the angular spread of the reading beam is approximately  $10^{-3}$  times the diffraction angle of the gratings. Figure 9(a) shows the simulated response for an apodized grating for reading beams of two different widths. The apodization was chosen to be a product of a sinc function and a Gaussian to achieve a flat peak response while maximizing side-mode suppression. As the spot diameter is reduced, the beam divergence increases, and the nulls in the grating response are smoothed while the peak diffraction efficiency is also reduced [Fig. 9(b)]. This effect explains the discrepancy between the simulated and experimental values of the peak diffraction efficiencies of the wavelength multiplexer in Fig. 7.

In conclusion, we have presented the design of a low through channel loss, compact wavelength multiplexer employing multiplexed gratings written in a photosensitive medium. The advantages and disadvantages of the multiple gratings written in the same region of the glass have been compared with isolated gratings. In testing the model, simulations and experiment compared favorably for an example two-channel wavelength multiplexer written in photosensitive silicate glass for use in wavelength division multiplexing applications at wavelengths of 1310 and 1550 nm with a diffraction efficiency  $>80\%$  and cross

talk of  $(-13.5 \pm 0.5)$  dB. Apodization is used to achieve a cross talk of  $<-30$  dB. All the multiplexers have a through channel loss of approximately 0.5 dB. A reduction in peak efficiency by  $<0.05$  dB can be expected owing to dispersion for a reading beam spot size of  $>2$  mm for the multiplexers described here.

Corresponding author Stephen R. Forrest can be reached at the Department of Electrical Engineering, Princeton University, B303, Engineering Quadrangle, Olden Street, Princeton, New Jersey 08540 or by phone, 609-258-4532; fax, 609-258-7272; or e-mail, forrest@princeton.edu.

## REFERENCES

1. Y. Hibino, "Recent advances in high-density and large-scale AWG multi/demultiplexers with higher index-contrast silica-based PLCs," *IEEE J. Sel. Top. Quantum Electron.* **8**, 1090-1101 (2002).
2. F. Cuesta, A. Griol, A. Martinez, and J. Marti, "Experimental demonstration of photonic crystal directional coupler at microwave frequencies," *Electron. Lett.* **39**, 455-456 (2003).
3. K. B. Chung and H. W. Hong, "Wavelength demultiplexers based on the superprism phenomena in photonic crystals," *Appl. Phys. Lett.* **81**, 1549-1551 (2002).
4. T. Erdogan and V. Mizrahi, "Thin-film filters come of age," *Photonics Spectra* **37**, 94-100 (2003).
5. T. Honda, A. Liu, J. Valera, J. Colvin, K. Sawyer, and R. McLeod, "Diffraction compensated free space WDM add-drop module with thin film filters," *IEEE Photonics Technol. Lett.* **15**, 69-71 (2003).
6. W. Tong, V. M. Menon, F. Xia, and S. R. Forrest, "An asymmetric twin-waveguide eight channel polarization independent arrayed waveguide grating with an integrated photodiode array," *IEEE Photonics Technol. Lett.* **16**, 1170-1172 (2004).
7. K. Sayano, H. E. Miller, B. Volodin, F. Zhou, and N. Karlovac, "Modular WDM add-drop multiplexers," *Proc. SPIE* **3234**, 102-107 (1997).
8. T. K. Gaylord and M. G. Moharam, "Planar dielectric grating diffraction theories," *Appl. Phys. B Photophys. Laser Chem.* **28**, 1-14 (1982).
9. H. Kogelnik, "Coupled wave theory for thick hologram gratings," *Bell Syst. Tech. J.* **48**, 2909-2947 (1969).
10. O. M. Efimov, L. B. Glebov, L. N. Glebova, K. C. Richardson, and V. I. Smirnov, "High-efficiency Bragg gratings in photothermorefractive glass," *Appl. Opt.* **38**, 619-627 (1999).
11. J. E. Pierson and S. D. Stookey, "Method for making photosensitive colored glass," U.S. patent 4,057,408 (1977).
12. N. F. Borelli, "Integral photosensitive optical device and method," U.S. patent 4,514,053 (1985).
13. S. Datta, C. Li, S. R. Forrest, B. Volodin, S. Dolgy, E. Melnik, and V. S. Ban, "Modeling of non-ideal volume Bragg reflection gratings in photosensitive glass using a perturbed transmission matrix approach," *IEEE J. Quantum Electron.* **40**, 580-590 (2004).
14. R. Freed, M. N. Zervas, and M. A. Muriel, "An efficient inverse scattering algorithm for the design of nonuniform fiber Bragg gratings," *IEEE J. Quantum Electron.* **35**, 1105-1115 (1999).
15. S. T. Hendow, "Crystal Bragg gratings stabilize laser sources," *Laser Focus World* **32**, S19-S24 (1996).
16. N. Kukhtarev, T. Kukhtareva, R. Jones, J. Wang, and P. Banerjee, "Real time holography for optical processing using photorefractive crystals," *Proc. SPIE* **3793**, 90-102 (1999).
17. S. Orlic, S. Ulm, and H. J. Eicher, "3D bit-oriented optical storage in photopolymers," *J. Opt. A Pure Appl. Opt.* **3**, 72-81 (2001).